



# Hydrogenolysis of cornstalk lignin in supercritical ethanol over N-doped micro-mesoporous biochar supported Ru catalyst

Bowen Luo<sup>a</sup>, Linxuan Zhou<sup>a</sup>, Zhipeng Tian<sup>a</sup>, Yao He<sup>b,\*</sup>, Riyang Shu<sup>a,\*</sup>

<sup>a</sup> Guangdong Provincial Key Laboratory of Functional Soft Condensed Matter, School of Materials and Energy, Guangdong University of Technology, Guangzhou 510006, PR China

<sup>b</sup> Institute of Environmental Health and Pollution Control, School of Environmental Science and Engineering, Guangdong University of Technology, Guangzhou 510006, China

## ARTICLE INFO

### Keywords:

Biochar  
N-doping  
micro-mesoporous  
Hydrogenolysis  
Lignin

## ABSTRACT

Biochar is a promising support to prepare metal-based catalysts due to its large surface area and special porous structure. This work proposed a novel Ru-based biochar catalyst by using KCl and melamine as templates to produce micro-mesoporous structure and realize N-doping at the same time. The prepared Ru/NMC catalyst showed a good hydrogenolysis performance of cornstalk lignin in supercritical ethanol. A series of catalyst characterizations were carried out to reveal the effects of micro-mesoporous structure and N-doping on the lignin hydrogenolysis. The micro-mesoporous structure led to a large surface area, which favored the dispersion of metal site and facilitated the mass transfer and diffusion during lignin hydrogenolysis, while the N-doping formed abundant edge N atoms, which promoted the interaction and the electron transfer between the loaded Ru and the support. These two crucial factors synergistically improved the lignin hydrogenolysis, with 31.2 wt% monomer yield at the reaction temperature of 260 °C.

## 1. Introduction

High-speed economic development causes the energy crisis, and the overuse of fossil resources results in the environmental pollution. It is urgent to search for a green and renewable energy to replace fossil resources [1]. As a renewable carbon source, biomass has attracted much attention due to its rich reserves, low cost and wide distribution in nature [2]. Lignocellulose biomass is the most kind of biomass, which consists of cellulose, hemicellulose and lignin [3]. The conversion of lignocellulose biomass is promising to produce sustainable chemicals and fuels due to its high-carbon and low-sulfur elementary composition [4,5]. Compared with cellulose and hemicellulose, lignin possesses a more complex structure and a higher bond dissociation energy that limits its depolymerization utilization efficiency [6]. Thus, lignin is commonly a biorefinery waste combusted directly for heat, which results in resource loss and environmental pollution.

Lignin is the only kind of renewable source that naturally contains aromatic units [7]. It is formed primarily from random ligation of coniferyl alcohol (G), sinapyl alcohol (S), and p-coumaryl alcohol (H) phenylpropane units by C—O and C—C bonds [8]. Selective breaking of these linked bonds can convert lignin into aromatic oligomers, dimers,

monomers and their derivatives, which are regarded as significant sources for further upgrading to produce valuable chemicals or liquid fuels [9,10]. Therefore, the valorization of lignin significantly relies on the efficient breakage of the C—O and C—C bonds. There are various strategies of lignin depolymerization [11], including hydrolysis, hydrogenolysis, oxidation [12], etc., wherein hydrogenolysis is considered as one of the most efficient processing ways to depolymerize lignin into low oxygen content and stable compounds [13–15]. Metal-based catalysts have been widely used due to their good chemical, thermal and mechanical stability [16]. Noble metal and transition metal are the common choices for the catalysis of lignin hydrogenolysis. Among the noble metal catalysts, Ru is the most used catalysts because of its relatively low cost and high catalytic activity in producing aromatic monomers [17,18]. In addition to the metal site, the catalyst support also enables to the improvement of lignin hydrogenolysis by regulating the metal loading dispersion and the interaction between the loaded metal and the support. Carbon materials, zeolites and metal organic frameworks (MOFs) are typical catalyst supports [19–22], and biochar derived from biomass waste possesses several advantages such as wide-spreading and low-cost, which has great potential in a wide range of industrial applications [23,24]. However, biochar often suffers from the

\* Corresponding authors.

E-mail addresses: [y.he@gdut.edu.cn](mailto:y.he@gdut.edu.cn) (Y. He), [shuriyang@gdut.edu.cn](mailto:shuriyang@gdut.edu.cn) (R. Shu).

<https://doi.org/10.1016/j.fuproc.2022.107218>

Received 29 November 2021; Received in revised form 23 January 2022; Accepted 18 February 2022

Available online 8 March 2022

0378-3820/© 2022 Elsevier B.V. All rights reserved.

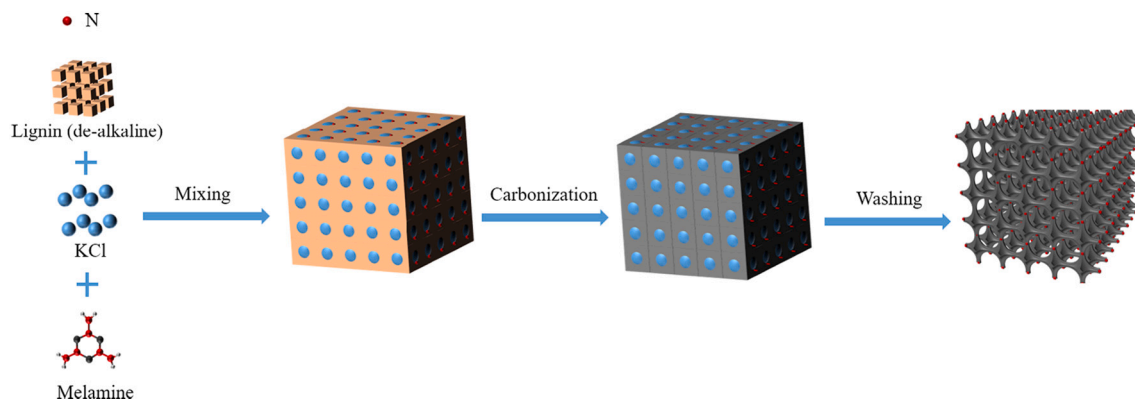


Fig. 1. Schematic illustration of the synthesis of NMC biochar using KCl and melamine as the templates.

blockage of the pore structure, and the biochar-based catalyst usually has the disadvantage of weak interactions between the loaded metal particle and the carbon support, resulting in the aggregation or leaching of the metal particles [25–27].

To enhance the interaction, N-doping is specifically applied into the carbon support. The formation of chemical bond between metal atoms and N atoms can accelerate electron transfer and improve the hydrogenolysis performance during the reaction process. Hu et al. reported the hydrogenolysis of lignin model compound over RuNi catalyst that loaded on a N-doped activated carbon (NC). The incorporation of N atoms favored the stability of metal particles and improved the hydrogenolysis activity [28]. Li et al. reported a Ru@N-doped carbon catalyst prepared in situ using a two-step method (pyrolysis of the mixture of metal, carbon, and N precursors). This catalyst presented a high catalytic efficiency on the cleavage of C—O bonds between lignin fragments, with a high total aromatic monomer yield [29]. The N-doped biochar support can anchor the metal nanoparticles effectively, while it commonly suffers from the poor pore volume and small surface area, which significantly limits the high dispersion of metals.

In this work, we proposed a new strategy to prepare the biochar support that realized N-doping and pore creation at the same time, which facilitated the high dispersion of Ru metal particles. The biochar derived from lignin waste pyrolysis, and ethylene glycol reduction was used to load the Ru metal on the N-doped micro-mesoporous carbon (NMC) support. The obtained Ru/NMC catalyst was employed for the hydrogenolysis of cornstalk lignin through lignin-first fractionation and exhibited good catalytic performance with high yield of monomer products.

## 2. Materials and methods

### 2.1. Materials

Cornstalk collected in Mengcheng, Anhui Province, China, was washed and dried at 60 °C for 48 h, screened for 30-mesh. The composition of the cornstalk feedstock, containing 70.9 wt% cellulose and hemicellulose, 24.3 wt% lignin and 4.8 wt% ash, was assessed under the National Renewable Energy Laboratory (NREL) procedure [30]. Chemical reagents were purchased from various reagent suppliers as following: RuCl<sub>3</sub> (Aladdin Chemical Reagent Co. Ltd), KCl, melamine and dealkaline lignin (Macklin Reagent), and other chemicals including ethanol, ethylene glycol, tetrahydrofuran (Damao Company).

### 2.2. Catalyst synthesis and characterization

As shown in Fig. 1, the biochar supported metal catalyst was typically synthesized as following procedures taking NMC biochar as an example. 2.0 g of dealkaline lignin, 0.5 g of the salt template KCl and 0.5 g N source melamine were fully mixed with mortar and pestle. The

mixture was transferred to the tube furnace with a constant nitrogen flow (60 mL/min) and underwent pre-carbonization (30–300 °C, 3 °C/min; heating for 1 h) and high-temperature carbonization (300–700 °C, 1 °C/min; heating for 2 h). The carbonized product was washed three times with deionized water and ethanol, and then vacuum dried at 60 °C to obtain NMC biochar support. The same procedure was conducted to prepare MC and NC biochar with adding KCl and melamine respectively. Conventional C biochar was prepared by dealkaline lignin pyrolysis without any template addition.

Ethylene glycol (EG) reduction method was employed to produce Ru-based biochar catalyst. Typically, 2.5 mL of RuCl<sub>3</sub> aqueous solution (including 0.05 g metal Ru), 1 g of biochar support and 30 mL of EG were added to a 50 mL 316 L autoclave. The reactor was filled with nitrogen, and then heated to 200 °C for 2 h under the stirring rate of 400 r/min. After the reaction, the mixture was centrifuged at 10000 r/min and washed three times with ethanol. Finally, the samples were dried by vacuum overnight at 40 °C.

Element analyzer (Vario EL III) was applied to determine the contents of C, H and N elements of the biochar samples. Scanning electron microscope (SEM, Hitachi Su8010) measurement was conducted to observe the morphology of the biochar samples, coupled with an Energy Dispersive Spectrometer (EDS) to exam the element distribution. Raman spectra were measured on a Raman microscope (LabRAM HR800, France) using 532 nm laser excitation at ambient temperature. The adsorption-desorption isotherm of nitrogen was determined by a Micromeritics ASAP 2010 instrument with a temperature set to -196 °C, and specific surface area and micropore volume ( $V_{mic}$ ) of the catalysts were calculated by Brunauer-Emmett-Teller (BET) and t-plot method, respectively. Pore diameter distribution was calculated by the Barrett-Joyner-Halenda (BJH) method. The total pore volume ( $V_{tot}$ ) was determined by the N<sub>2</sub> adsorption-desorption curve at  $P/P_0 = 0.99$ , while the mesopore pore volume ( $V_{meso}$ ) was determined by the difference between  $V_{tot}$  and  $V_{mic}$ . Transmission electron microscope (TEM) measurement was performed on Jeol TEM-100CX. X-ray photoelectron spectroscopy (XPS) was measured with Thermo-VG Scientific ESCALAB 250 spectrometer.

### 2.3. Typical experiment of lignin hydrogenolysis and product analysis

The hydrogenolysis experiment of lignin was performed in a 50 mL stainless-steel autoclave (Anhui Kemi Instrument Co., Ltd.). Specifically, 0.5 g cornstalk, 0.2 g catalyst and 15 mL ethanol were added to the reactor. Then the autoclave was purged three times with hydrogen and charged in 1 MPa hydrogen pressure. Afterwards, the reactor was heated to 260 °C for 4 h under the stirring rate of 400 r/min. When the reaction finished, the reactor was cooled to room temperature to take out the product mixture. Every lignin hydrogenolysis experiment was repeated for three times and the average value was used for the results.

The reactor pressure before and after reaction did not change much,

**Table 1**  
Elemental analysis of the different biochars.

Samples	C (%)	H (%)	O <sup>a</sup> (%)	N (%)
C	84.8	1.7	12.8	0.6
MC	76.2	2.2	21.0	0.5
NC	77.6	2.2	12.1	8.0
NMC	70.4	2.3	22.7	4.5

<sup>a</sup> The oxygen content was estimated by the conservation of mass based on the assumption that the samples only contain C, H, N and O.

therefore the weight of the gas product was negligible. The separation procedure for the cornstalk hydrogenolysis products was conducted as following. Filtration was applied to separate the solid and liquid phase of the products. Then the solids that contained the retentive cellulose and hemicellulose, catalyst, and lignin residues were washed three times with ethanol and deionized water, and dried at 60 °C for 24 h. The dried solid was screened to 200-mesh for catalyst recycle. After catalyst removal, the residual solids were treated by H<sub>2</sub>SO<sub>4</sub> to eliminate the component of cellulose and hemicellulose and the lignin residues were obtained. The retention rate of cellulose and hemicellulose was calculated based on the weight change before and after H<sub>2</sub>SO<sub>4</sub> treatment, compared to the original weight in the cornstalk. At the end, the qualitative and quantitative analysis of the filtered liquid product were carried out. A part of the liquid product was diluted by ethanol to measure the volatile products, and the rest of the liquid product was evaporated in vacuum to obtain nonvolatile oligomer products. Then, the volatile products were analyzed, by gas chromatography–mass spectrometry (GC–MS, Thermo Fisher Scientific Trace 1300) equipped with column TG-5sil using acetophenone as the internal standard.

The GC oven was maintained at 60 °C for 2 min, risen to 260 °C at 10 °C/min and then kept for 10 min. The liquefaction degree of lignin and the yield of monomer product were evaluated according to Eqs. (1) and (2). The yield of the oligomers was calculated by mass balance from Eq. (3).

$$\text{Degree of liquefaction (\%)} = (W_F - W_R)/W_F \times 100\% \quad (1)$$

$$\text{Yield of the monomer products (\%)} = W_M/W_F \times 100\% \quad (2)$$

$$\text{Yield of the oligomers (\%)} = (W_F - W_M - W_R)/W_F \times 100\% \quad (3)$$

where  $W_F$  and  $W_R$  referred to the weight of lignin in the raw cornstalk and the weight of lignin residues, respectively.  $W_M$  was the weight of monomer products.

The molecular weight of nonvolatile products was determined by a gel penetration chromatography (GPC, the Agilent 1260 Infinity), using tetrahydrofuran (external calibration) as the flow phase. Elemental analysis was performed using a Vario EL III element analyzer. Fourier transform infrared spectroscopy (FT-IR) was employed using KBr pelleting method with Nicolet Is 50 FT-IR spectrometer.

### 3. Results and discussion

#### 3.1. Biochar supports and Ru-based biochar catalysts characterization

Element analysis was conducted to compare the biochars prepared by different procedures and templates. As shown in Table 1, the C biochar support showed that the contents of C, H, O and N were 84.8%, 1.7%, 12.8% and 0.6%, respectively. With the addition of KCl template during the preparation procedures, the obtained MC biochar presented an increase of O and a decrease of C, due to that the addition of KCl made the biochar a relative loose structure with the formation of micropore/mesopore. NC biochar prepared by the addition of melamine exhibited a significant increase of N element (8.0%), suggesting that nitrogen had been successfully introduced into the biochar structure. As for the NMC biochar sample, the N element content was also increased to 4.5%, although it was lower than that of NC biochar. This indicated that the micro-mesoporous structure of NMC biochar resulted in a loss of N element and an increase of O element.

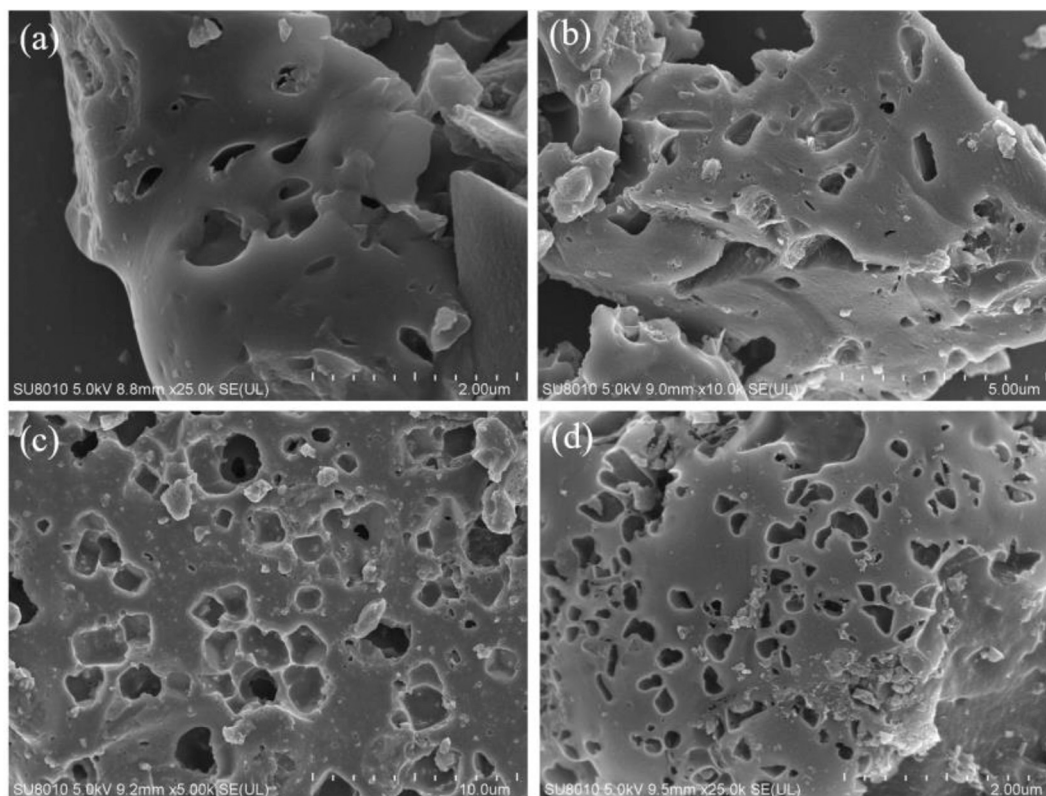


**Fig. 2.** SEM images of (a) C, (b) NC, (c) MC and (d) NMC biochar supports.

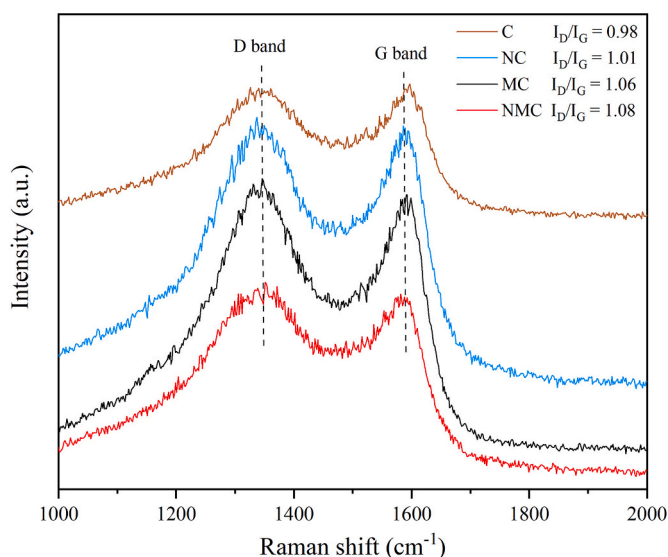


Fig. 3. Raman spectra of the different biochar supports.

Table 2  
Surface properties of the different catalysts.

Catalyst	Surface area <sup>a</sup> (m <sup>2</sup> g <sup>-1</sup> )	Pore diameter <sup>b</sup> (nm)	Pore volume <sup>c</sup> (cm <sup>3</sup> /g)			V <sub>mic</sub> / V <sub>tot</sub> (%)
			V <sub>tot</sub>	V <sub>mic</sub>	V <sub>meso</sub>	
Ru/C	7	13.6	0.01	–	–	–
Ru/NC	15	8.0	0.02	0.01	0.01	50.0
Ru/MC	745	5.7	0.33	0.28	0.05	84.8
Ru/ NMC	537	4.9	0.29	0.21	0.08	72.4

<sup>a</sup> MultiPoint Brunauer, Emmett & Teller (BET) method.

<sup>b</sup> Barrett, Joyner & Halenda (BJH) method.

<sup>c</sup> V<sub>tot</sub>: total pore volume was determined using density functional theory (DFT) method Boehm's titration. V<sub>mic</sub>: micropore volume was calculated using the t-plot method. V<sub>meso</sub>: mesopore volume was determined by the difference between the V<sub>tot</sub> and the V<sub>mic</sub>.

The different biochar supports were analyzed with SEM to compare their structure and morphology. As shown in Fig. 2a, the C biochar exhibited a relatively plain and porousless surface morphology, which indicated a small surface area and a small pore volume. NC biochar (Fig. 2b) had similar morphology to C biochar but was more porous. It was because that melamine as a nitrogen source also enabled the formation of a small amount of micropore/mesopore structures due to the thermal decomposition of melamine. MC biochar (Fig. 2c) presented an irregular porous surface structure, in which KCl acted as a salt template and resulted in the appearance of pores and defect sites during the pyrolysis process. Moreover, as shown in Fig. 2d, the surface of NMC biochar had an abundant porous structure. Combined the results of elemental analysis in Table 1, it can be concluded that NMC biochar took both advantage of MC and NC biochars, with a high amount of porous structure and a high amount of N-doping. Moreover, EDS mapping was also carried out to observe the element distribution. Results in Fig. S1 showed that there was a little amount of Cl and K still left in the NMC biochar although the sample has been washed with water for three times. It indicated that Cl and K were also introduced into the internal structure of the NMC biochar.

Raman spectra of the biochars were also presented to investigate the defect sites. As shown in Fig. 3, the D band (1350 cm<sup>-1</sup>) and G band (1580 cm<sup>-1</sup>) were two typical distinctive peaks in the Raman spectrum of carbon materials, in which the D band exhibited the structural irregularity at defect sites and the G band indicated the vibration of the sp<sup>2</sup> C–C bonds [29]. The I<sub>D</sub>/I<sub>G</sub> ratio revealed the graphitization degree

of the biochars. The I<sub>D</sub>/I<sub>G</sub> value of C biochar was 0.98, showing superior graphite structure. The addition of melamine template less changed the graphite structure in the case of NC biochar. After the introduction of KCl template, the I<sub>D</sub>/I<sub>G</sub> value in the case of MC biochar increased to 1.06, which indicated the formation of defect sites. Moreover, the NMC biochar exhibited the highest I<sub>D</sub>/I<sub>G</sub> value (1.08), demonstrating the large amount of the introduced defect sites in the carbon matrix. The defect sites further enabled the metal atoms to be anchored and promoted the metal dispersion during the reduction processing.

To confirm the abundant micro-mesoporous structure of NMC biochars, BET measurement was also conducted. The N<sub>2</sub> adsorption-desorption isotherms of the prepared catalysts were displayed in Fig. S2. It can be seen clearly that Ru/C and Ru/NC catalysts presented a small amount of N<sub>2</sub> adsorption, while Ru/MC and Ru/NMC catalysts exhibited a relative high one, referring to abundant porous structure. Besides, when the relative pressure was above 0.4, all catalysts showed hysteresis loops (type IV), which proved the presence of mesopores. At the stage of relative pressure below 0.4, the adsorption volumes in the cases of Ru/MC and Ru/NMC catalysts increased dramatically in the pattern of type I, confirming the presence of microporous structure. BET results were listed in Table 2 to compare the different Ru-based biochar catalysts. Ru/C biochar catalyst exhibited a poor surface area and a low pore volume, probably due to the highly condensation structure of the dealcaline lignin. After melamine addition, the surface area of Ru/NC was increased to 15 m<sup>2</sup>/g and the pore diameter was decreased to 8.0 nm. The pore volume also slightly increased, with the formation of micropores and mesopores. With the addition of KCl to form Ru/MC catalyst, the surface area and the pore volume were sharply increased to 745 m<sup>2</sup>/g and 0.33 cm<sup>3</sup>/g, respectively. Meanwhile, micropore structure was greatly developed in Ru/MC, with the enhanced V<sub>mic</sub>/V<sub>tot</sub> ratio of 84.8%. As for Ru/NMC catalyst, the surface area was 537 m<sup>2</sup>/g and the pore volume was 0.29 cm<sup>3</sup>/g, both of which were slightly lower than that of Ru/MC catalyst, and the V<sub>mic</sub>/V<sub>tot</sub> ratio decreased to 72.4%. It indicated that the N-doping procedure would slightly suppress the formation of micro-mesoporous structure.

TEM measurements were carried out to compare the metal dispersion of the different Ru-based biochar catalysts. It was found that the Ru metal particles were uniformly distributed on the Ru-based biochar catalysts (Fig. 4). The Ru/C, Ru/NC and Ru/MC catalysts presented an average Ru metal particle size of 3.5, 3.3 and 3.2 nm, respectively. Comparatively, Ru/NMC catalyst showed a smaller Ru metal particle size of 2.8 nm. Obviously, N-doping and micro-mesoporous structure greatly improved the dispersion of metal sites. The decrease of the Ru metal particle size can result in higher catalytic activity. The reason for this can be that N-doped biochar support enhanced the electron interaction between the metal and the support, and therefore promoted the reduction of Ru metal and the dispersion of Ru metal particles [29]. Moreover, the micro-mesoporous structure of the catalysts led to a large surface area, which can provide more sites for the Ru metal dispersion.

XPS measurements were also investigated to reveal the interaction between Ru and supports, as well as the N species (Fig. S3, Fig. 5 and Fig. S4). The O 1s peaks corresponded to the peaks assigned to C=O, C–OH and O=C–O bonds [31,32], which indicated the abundance of the different groups on the surface of biochars. The C 1s peaks of the different Ru-based biochar catalysts were deconvoluted into four peaks (Fig. 5a), corresponding to the binding energy of 284.8, 285.3, 286.2 and 289.1 eV for the C–C/C=C, C–O/C–N, C=O and COOH, respectively [31,32]. An increased percentage of total C–N atoms was presented in Ru/NC and Ru/NMC catalysts compared to Ru/C and Ru/MC catalysts, which indicated the effective incorporation of N elements by the addition of melamine [33]. Ru 3d XPS spectra was also showed in Fig. 5a. The presence of the peaks around 280.3 eV demonstrated the existence of Ru<sup>0</sup> species [34]. And the binding energy of Ru 3d<sub>5/2</sub> moved to a low binding energy position in the order of Ru/C (280.8 eV) > Ru/NC (280.6 eV) > Ru/MC (280.4 eV) > Ru/NMC (280.3 eV), suggesting that the introduced N atoms supplied electrons to the Ru metal. Ru 3p

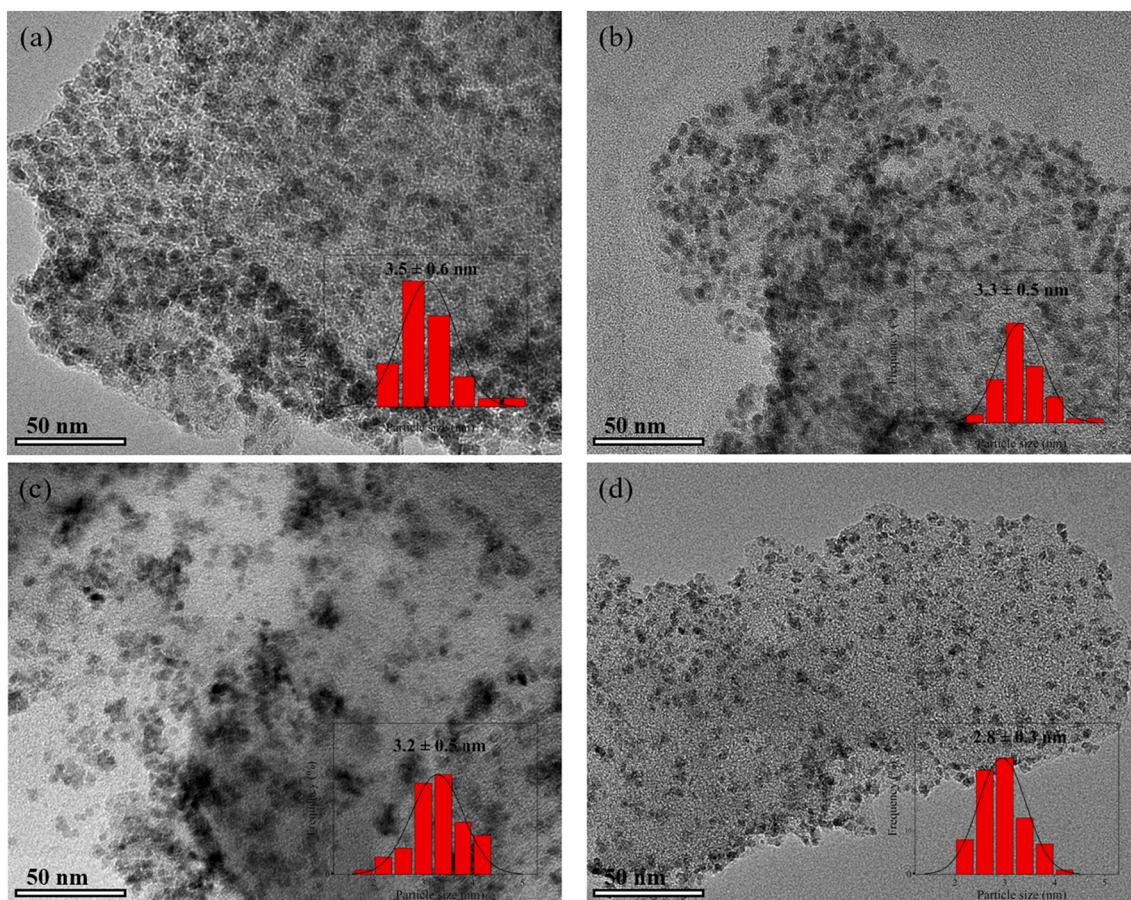


**Fig. 4.** TEM images of the different Ru-based biochar catalysts (a) Ru/C, (b) Ru/NC, (c) Ru/MC, and (d) Ru/NMC. The mean Ru diameter was estimated using  $d_{\text{TEM}} = \sum n_i d_i^3 / \sum n_i d_i^2$ , where  $n_i$  is the number of metal having diameter  $d_i$  ( $n > 200$ ).

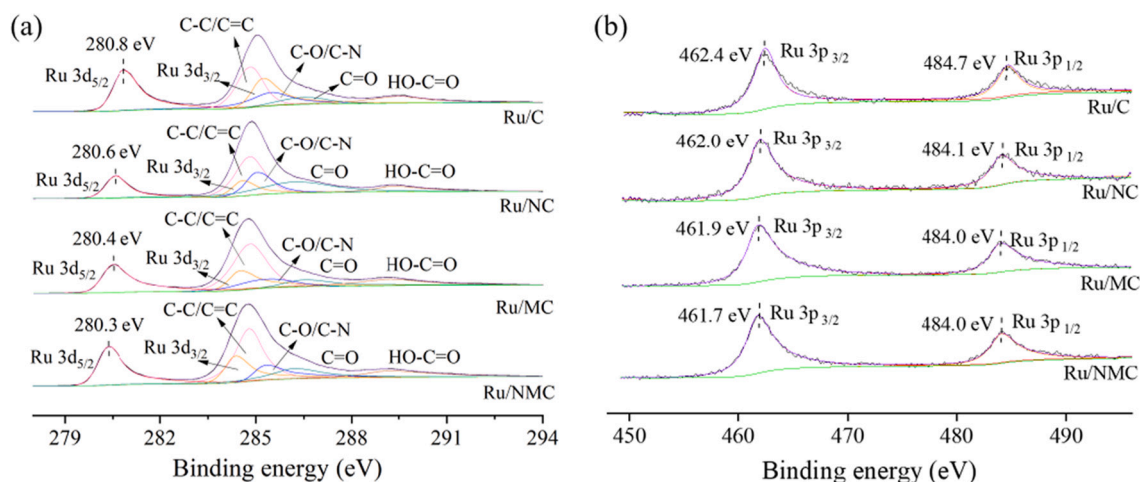


**Fig. 5.** The deconvoluted XPS spectra of (a) Ru 3d and (b) Ru 3p of different Ru-based biochar catalysts.

XPS spectra also had two different peaks, with the binding energy of around 462.4 eV and 484.7 eV (Fig. 5b). Similar to the Ru 3d<sub>5/2</sub> spectra, the binding energy of Ru 3p<sub>3/2</sub> and Ru 3p<sub>1/2</sub> decreased in the order of Ru/C > Ru/NC > Ru/MC > Ru/NMC. It also confirmed the interaction and the electron transfer between Ru and supports. This interaction favored the stability of metal particles, which was also conducive to the high dispersion of Ru metal that presented in Fig. 4. In addition, the micro-mesoporous structure of Ru/NMC catalysts not only contributed to metal dispersion but also increased the defect sites of N on the support

to enhance the electron migration between N atoms and Ru atoms [35].

The high resolution XPS spectra of N 1s of Ru/NC and Ru/NMC catalyst were also explored and the results were presented in Fig. S4. The XPS spectrum of N 1s was deconvoluted into four major peaks at 398.2 eV, 399.8 eV, 401.1 eV and 402.5 eV, belonging to pyridine N (N-6), pyrrole N (N-5), graphitic N (N-Q), and nitrogen oxide, respectively [36]. It was found that the extra addition of KCl template changed the distribution of N species. Ru/NMC catalyst had decreased N-Q content and increased N-6 content compared to Ru/NC catalyst, and its N-5

**Table 3**  
Effect of catalysts on lignin hydrogenolysis and product distribution.

Entry	Catalyst	Liquefaction (%)	Monomers (wt%)					Oligomers (wt%)
			Phenols	Guaiacols	Syringols	Hydrogenated products	Total	
1	None	38.1 ± 3.5	2.1 ± 0.5	0.7 ± 0.2	2.0 ± 0.3	0.4 ± 0.1	5.2 ± 1.0	32.9 ± 2.5
2	Ru/C	73.5 ± 2.2	7.7 ± 0.6	8.2 ± 0.5	1.0 ± 0.2	2.8 ± 0.7	19.7 ± 1.4	53.8 ± 0.8
3	Ru/NC	76.1 ± 2.5	11.2 ± 0.7	10.6 ± 0.8	0.8 ± 0.4	0.7 ± 0.3	23.3 ± 1.2	52.8 ± 1.3
4	Ru/MC	78.2 ± 1.8	9.7 ± 0.6	12.1 ± 1.0	0.2 ± 0.1	3.3 ± 0.5	25.1 ± 0.8	53.1 ± 1.0
5	Ru/NMC	80.7 ± 2.2	15.0 ± 1.2	13.7 ± 0.8	0.7 ± 0.2	1.8 ± 0.6	31.2 ± 1.0	49.5 ± 1.2

Condition: 0.5 g cornstalk, 0.2 g catalyst, 15 mL ethanol, 1 MPa H<sub>2</sub>, 260 °C, 4 h.

**Table 4**  
Comparison of different catalysts on the hydrogenolysis of lignin.

Catalysts	Reaction condition	Hydrogenolysis efficiency		Ref.
		Liquefaction	Products	
Ni/C (biochar derived from extracted lignin)	300 °C, 5 h, 1 MPa H <sub>2</sub>	91.0%	7.0 wt% yield of phenols	[38]
Ni-Co/C (biochar derived from rice straw)	280 °C, 15 min	72.0%	18.2 wt% yield of phenolic monomers	[39]
Ni-MgAlO/C (biochar derived from sodium ligninsulfonate)	200 °C, 6 h, 1 MPa H <sub>2</sub>	–	22.0 wt% total mass yields of aromatics	[40]
Ni/C (biochar derived from extracted lignin)	260 °C, 10 h, 1 MPa H <sub>2</sub>	87.4%	23.3 wt% yield of aromatic monomers	[41]
Pd-Al <sub>2</sub> O <sub>3</sub> /C (biochar derived from plastic and biomass)	240 °C, 3 h, 3 MPa H <sub>2</sub>	70.4%	30.0 wt% yield of C9 monomeric guaiacols	[42]
Ni-Mo <sub>2</sub> C/C (biochar derived from sawdust)	250 °C, 2 h, 2 MPa H <sub>2</sub>	61.3%	31.9 wt% yield of aromatic monomers	[43]
Ru/NMC (biochar derived from dealkaline lignin)	260 °C, 4 h, 1 MPa H <sub>2</sub>	80.7%	31.2 wt% yield of aromatic monomers	This work

content essentially kept unchanged. N-Q had little effect on the catalytic performance due to its stable chemical property. N-6 and N-5 species both belonged to edge N atoms, which enabled the stabilization of the Ru particles because their lone-pair electrons can serve as metal coordination sites [21]. The incorporated N-6 can also tune the electronic density of Ru particles and increase metal sites through the electronic interactions [37]. Overall, the edge N atoms in NMC significantly

promoted the electron transfer between Ru and supports.

### 3.2. Catalytic performance of cornstalk lignin hydrogenolysis

As shown in Table 3, different Ru-based biochar catalysts exhibited different hydrogenolysis activity on the cornstalk lignin fractionation in supercritical ethanol. The volatile products mainly consisted of guaiacols, phenols, syringols and hydrogenated products. Without catalyst addition, the lignin liquefaction degree and the monomer yield were 38.1% and 5.2 wt% respectively, indicating the occurrence of lignin alcoholysis. With the addition of Ru-based biochar catalysts, the lignin hydrogenolysis performance was improved significantly. Ru/C catalyst showed a lignin liquefaction degree of 73.5% and a monomer yield of 19.7 wt%. Particularly, in the use of N-doped Ru/NC catalyst, the monomer yield increased to of 23.3 wt%, indicating that the N-doping had a positive effect on the lignin hydrogenolysis. The interaction between Ru and N proved by TEM measurement (Fig. 4) and XPS spectra (Fig. 5) was mainly responsible for this improvement. Ru–N interaction contributed to uniform dispersion of the Ru particles on the carbon support and prevented them against aggregation, and the highly dispersed Ru-based catalyst presented a high catalytic activity. Moreover, the incorporated nitrogen atoms could also donate electrons to the loaded Ru metal and improve the lignin hydrogenolysis activity [29]. The Ru/MC catalyst obtained a higher monomer yield of 25.1 wt%, due to that the large specific surface area and the abundant microporous structure enhanced the metal dispersion and facilitated the mass transfer and diffusion during lignin hydrogenolysis. Moreover, Ru/NMC catalyst showed the best lignin hydrogenolysis performance, with the lignin liquefaction degree and the monomer yield up to 80.7% and 31.2 wt% respectively. Ru/NMC catalyst possessed both the advantages of Ru/NC and Ru/MC catalysts, including the abundant microporous structure and the interaction between Ru and N. Meanwhile, the catalytic performance of Ru/NMC also suggested that small Ru metal particle size enabled the improvement of hydrogenolysis

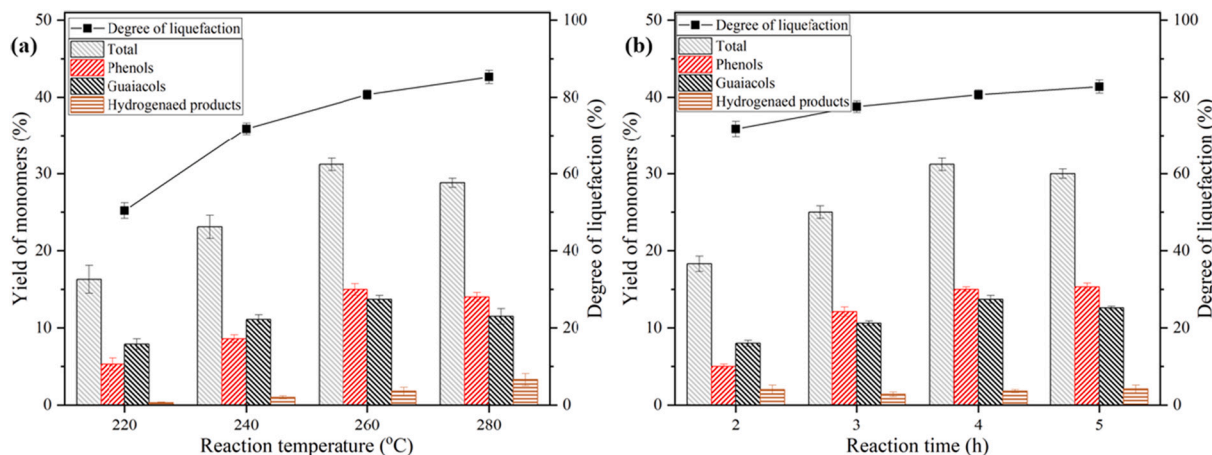


**Fig. 6.** Effects of (a) reaction temperature and (b) time on the lignin hydrogenolysis and yield of monomer products. Condition: (a) 0.5 g cornstalk, 0.2 g Ru/NMC catalyst, 15 mL ethanol, 1 MPa H<sub>2</sub>, 4 h. (b) 0.5 g cornstalk, 0.2 g Ru/NMC catalyst, 15 mL ethanol, 1 MPa H<sub>2</sub>, 260 °C.

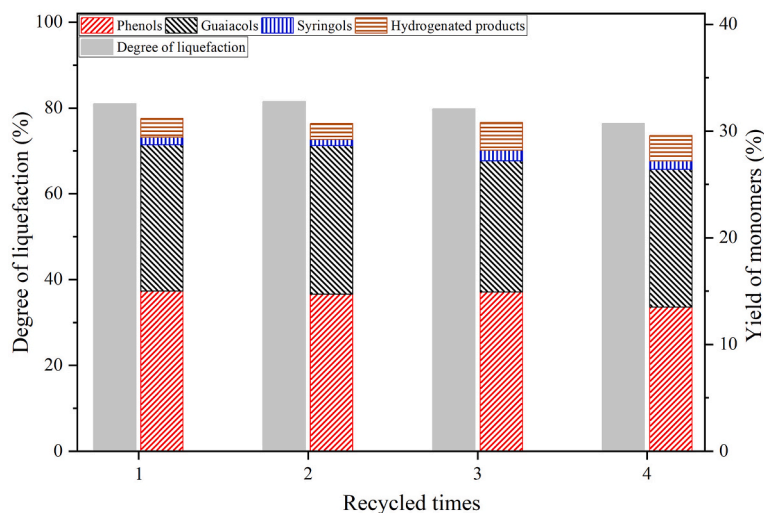


Fig. 7. The recyclability of the Ru/NMC catalyst. Condition: 0.5 g cornstalk, 0.2 g catalyst, 15 mL ethanol, 1 MPa H<sub>2</sub>, 260 °C, 4 h.

Table 5

Average molecular weight of the nonvolatile products with different catalysts.

Catalyst	M <sub>n</sub> <sup>a</sup>	M <sub>w</sub> <sup>a</sup>	M <sub>z</sub> <sup>a</sup>	D <sup>a</sup>
Ru/C	431	972	2122	2.26
Ru/NC	372	783	1788	2.10
Ru/MC	402	806	1770	2.02
Ru/NMC	347	684	1720	1.97

<sup>a</sup> M<sub>n</sub>: number average molecular weight; M<sub>w</sub>: weight average molecular weight; M<sub>z</sub>: Z-average molecular weight; D: dispersion degree.

activity. The presence of edge N atoms and Ru–N interactions were key to prevent Ru nanoparticles from agglomeration.

The product distribution was also investigated in detail in order to compare the catalytic effect of different Ru-based biochar catalysts. GC–MS results (Table S1 and Fig. S5) identified every component of the volatile products, including phenols, guaiacols, syringols and hydrogenated products. It can be seen that the N-doped catalysts (Ru/NC and Ru/NMC) produced phenols as the major products, while the catalysts without N-doping (Ru/C and Ru/MC) produced guaiacols as the major products. This difference was mainly resulted from the occurrence of demethoxylation reaction that were promoted by increasing acid sites from the N-doping treatment. In order to confirm the good demethoxylation performance of the N-doped catalysts, 4-propyl guaiacol was used as the model compound for hydrogenolysis. Results in Table S2 showed that the conversions were generally lower than that in cornstalk lignin hydrogenolysis, following the order Ru/NMC > Ru/MC > Ru/NC > Ru/C. The –OCH<sub>3</sub> containing products from N-doped biochar catalysts (Ru/NC and Ru/NMC) were much less than the case over N-doped catalysts (Ru/C and Ru/MC). The model compound study result was in good line with the hydrogenolysis results in Table 3. Moreover, the

Table 6

The main elements of nonvolatile products from lignin hydrogenolysis.

Catalyst	Elemental content				H/C ratio	O/C ratio	Experimental molecular formula	HHV <sup>b</sup> (MJ kg <sup>-1</sup> )	Degree of unsaturation <sup>c</sup>
	C	H	O <sup>a</sup>	N					
Ru/C	62.9	7.6	28.3	1.1	1.44	0.34	C <sub>9</sub> H <sub>13.00</sub> O <sub>3.04</sub> N <sub>0.14</sub>	27.00	3.57
Ru/NC	65.4	7.9	25.4	1.2	1.45	0.29	C <sub>9</sub> H <sub>13.06</sub> O <sub>2.62</sub> N <sub>0.14</sub>	28.86	3.54
Ru/MC	65.7	7.9	25.3	1.1	1.45	0.29	C <sub>9</sub> H <sub>13.03</sub> O <sub>2.60</sub> N <sub>0.13</sub>	28.98	3.55
Ru/NMC	68.1	8.4	22.2	1.2	1.49	0.24	C <sub>9</sub> H <sub>13.38</sub> O <sub>2.20</sub> N <sub>0.14</sub>	31.07	3.38

<sup>a</sup> The oxygen content was estimated by the conservation of mass based on the assumption that the samples only contain C, H, N and O.

<sup>b</sup> Evaluated by Dulong formula: HHV (MJ kg<sup>-1</sup>) = 0.3383 × C + 1.422 × (H–O/8).

<sup>c</sup> Evaluated by experimental molecular formula: Degree of unsaturation = (2C + 2–H–N)/2.

retention rate of cellulose and hemicellulose over different catalysts was also measured after hydrogenolysis process and the results were exhibited in Table S3. Ru/C had the highest retention rate of cellulose and hemicellulose, with the value of 86.5%. The retention rate in the case of Ru/MC was also as high as 78.4%, and the N-doped catalysts, Ru/NC and Ru/NMC had a little lower retention rate of 76.1% and 71.3%, respectively. It indicated that the N-doping promoted the conversion of cellulose and hemicellulose in supercritical ethanol.

The catalytic performance of lignin hydrogenolysis over the Ru/NMC catalyst in this work was compared with other biochar catalysts reported previously, as listed in Table 4. Biochar is a renewable material that derived from biomass waste. Therefore, it presents a great potential on the industrial application for its low cost. Previous results showed that the Ni/C catalyst derived from extracted lignin obtained 91% lignin liquefaction degree at the temperature of 300 °C, while the phenols yield was only 7.0 wt% [38]. Ni–Co/C catalyst derived from rice straw had a little higher yield of phenolic monomers (18.2 wt%) [39]. Ni–MgAlO/C catalyst derived from sodium ligninsulfonate achieved 22.0 wt% total mass yields of aromatics at the temperature of 200 °C, while the reaction time was as long as 6 h [40]. Another Ni/C catalyst derived from extracted lignin obtained 23.3 wt% yield of aromatic monomers at 260 °C after 10 h reaction [41]. Comparatively, the noble metal catalysts had a better catalytic performance than Ni catalysts. Pd–Al<sub>2</sub>O<sub>3</sub>/C catalyst derived from plastic and biomass exhibited 30.0 wt% yield of C<sub>9</sub> monomeric guaiacols [42]. Ni–Mo<sub>2</sub>C catalyst derived from sawdust presented 31.9 wt% yield of aromatic monomers due to that Mo<sub>2</sub>C possessed a similar catalytic property with noble metals [43]. In this work, Ru/NMC catalyst derived from dealkaline lignin showed 31.2 wt% yield of aromatic monomers at the reaction temperature of 260 °C, which demonstrated the superior performance of this catalyst.

The effect of reaction temperature and time on the catalytic hydrogenolysis of cornstalk lignin over Ru/NMC catalyst was investigated and

the results were showed in Fig. 6. Reaction temperature showed a positive correlation with lignin liquefaction degree (Fig. 6a). At the temperature of 220 °C, the lignin liquefaction degree and the monomer yield were only 50.4% and 16.3 wt%. The poor hydrogenolysis efficiency at low reaction temperature was probably due to the high reaction activation energy of C–O cleavage. With the increase of the temperature, the lignin hydrogenolysis performance was promoted greatly. At the temperature of 260 °C, the yield of monomer products reached the highest (31.2 wt%). When the temperature further increased, the lignin liquefaction degree still rose up gradually, but the yield of monomer products exhibited a slight downtrend. The excessive high reaction temperature promoted the condensation of active monomer products to form oligomers and resulted in a decrease of monomer yield. Reaction time also had a similar effect to reaction temperature on the lignin hydrogenolysis and product distribution (Fig. 6b). With the prolonging reaction time, lignin liquefaction degree was increased gradually from 71.8% to 83.5% in the range of 2–5 h, and the monomer yield was firstly improved to the maximum value of 31.2 wt% at 4 h, then dropped down to 29.8 wt% at 5 h. Prolonged reaction time intensified the condensation of active monomer products to form oligomers. Moreover, it can be noted that the yield of phenols increased with the prolonging reaction time. It indicated that part of the formed guaiacols were converted to phenols through demethoxylation procedures. Longer reaction time made this transformation more fully and resulted in more phenol products.

The recycled performance of the Ru/NMC catalyst was evaluated. After the reaction, the catalyst was separated, cleaned and then directly reused for the next reaction cycle. The result in Fig. 7 showed that this catalyst can be reused at least 4 times, with no significant loss in lignin hydrogenolysis efficiency. Only slightly drops of 4.5% in lignin liquefaction degree and of 1.6 wt% in monomer yield were observed after the fourth run. It indicated a high stability of the Ru/NMC catalyst. To investigate the reason for the small loss of hydrogenolysis efficiency, the fresh and spent Ru/NMC catalysts were compared by TEM characterization. Results in Fig. S6 showed that the spent catalyst formed several metal particle aggregation, which was the main reason for the drops in lignin liquefaction degree and monomer yield.

### 3.3. Analysis of the nonvolatile products

To compare the property of the nonvolatile products over different Ru-based biochar catalysts, the GPC measurement was employed to analyze the molecular weight of the nonvolatile products derived from lignin hydrogenolysis (Table 5). The results showed that when lignin hydrogenolysis occurred in the presence of Ru/C, the nonvolatile products had a large average molecular weight ( $M_w$ ) of 972 g/mol. Ru/MC catalyst showed a  $M_w$  value of 806 g/mol for the nonvolatile products. As for Ru/NC catalyst, a much lower  $M_w$  was presented (783 g/mol), indicating the good depolymerization capability of the N-doped catalyst. When the Ru/NMC was used as the catalyst, the value of  $M_w$  decreased to 684 g/mol, and the peak in the molecular weight range of 400–1200 g/mol became much smaller (Fig. S7). These results showed that Ru/NMC catalyst had the best depolymerization effect on the cornstark lignin, which was also in good line with the analysis of volatile products (Table 1). As for the dispersion degree, Ru/NMC catalyst was the lowest, indicating that the nonvolatile products possessed a concentrated distribution, which further confirmed the good catalytic activity of Ru/NMC catalyst.

The non-volatile products were also measured by FT-IR characterization. The four different sample had similar spectra, with slight difference in some functional groups (Fig. S8). The peaks of 3429  $\text{cm}^{-1}$  and 1216  $\text{cm}^{-1}$  correspond to the O–H vibration of the phenolic compounds [44], and the peaks of 1725  $\text{cm}^{-1}$  and 1606  $\text{cm}^{-1}$  correspond to the carboxyl group stretching and the structural vibration of the benzene rings, respectively [45]. The nonvolatile products formed by Ru/NMC catalysis had a relative larger peaks of phenolic compounds and benzene

structure, indicating the better hydrogenolysis performance of the catalyst. This also confirmed that the effects of the large surface area and the N-doping of the Ru/NMC catalyst contributed to the enhancement of lignin hydrogenolysis performances.

To further determine the composition of the nonvolatile products, elemental analysis was also performed. The results in Table 6 showed that the nonvolatile products derived from Ru/C catalyst had a high oxygen content (28.3%), with a low HHV values. And the samples obtained from the catalysis over Ru/NC and Ru/MC exhibited similar elemental composition. Particularly, the nonvolatile products from the Ru/NMC catalyst had the lowest oxygen content (22.2%) and the highest HHV value (31.07  $\text{MJ kg}^{-1}$ ). This suggests that the lignin hydrolysis process was strongly facilitated by the strong interaction of the highly dispersed metal Ru and a large number of edge N atoms. At the same time, a good deoxygenation efficiency was also achieved. Moreover, the product sample from the Ru/NMC catalysis had the lowest degree of unsaturation, indicating the strong ability of the Ru/NMC catalyst for hydrogenation, which was resulted from the highly dispersed Ru metal particles.

## 4. Conclusion

This study prepared a novel Ru-based biochar catalyst by using KCl and melamine as templates to create micro-mesoporous structure and realize N-doping. The obtained Ru/NMC catalyst exhibited a high catalytic activity on the hydrogenolysis of cornstark lignin, which was much better than Ru/C, Ru/NC and Ru/MC catalysts. The catalysts were characterized by element analysis, SEM, BET, TEM and XPS in detail. Results showed that micro-mesoporous structure and edge N atoms of the biochar support of Ru/NMC were the crucial factors for its superior catalytic performance. The micro-mesoporous structure can provide a large surface area, which favored the dispersion of metal particles and facilitated the mass transfer and diffusion during lignin hydrogenolysis. The N-doping led to abundant edge N atoms, which promoted the interaction and the electron transfer between Ru and biochar supports. Over the Ru/NMC catalyst, cornstark lignin was efficiently hydrogenolysed at a low temperature of 260 °C, affording 31.2 wt% monomer yield. Furthermore, the Ru/NMC had a good recyclability and can be used 4 times without significant activity loss.

### CRediT authorship contribution statement

**Bowen Luo:** Investigation, Methodology, Writing – original draft, Formal analysis, Visualization. **Linxuan Zhou:** Investigation, Methodology, Visualization, Validation. **Zhipeng Tian:** Formal analysis, Validation. **Yao He:** Writing – review & editing, Supervision, Funding acquisition. **Riyang Shu:** Conceptualization, Investigation, Writing – review & editing, Supervision, Funding acquisition.

### Declaration of Competing Interest

None.

### Acknowledgments

The authors gratefully acknowledge the financial support of the National Key Technology R&D Program of China (No. 2018YFB1501601) and the National Natural Science Foundation of China (No. 51806040).

### Appendix A. Supplementary data

Supplementary data to this article can be found online at <https://doi.org/10.1016/j.fuproc.2022.107218>.

## References

- [1] B. Jiang, L. Li, Z.F. Bian, Z.W. Li, M. Othman, Z.H. Sun, D.W. Tang, S. Kawi, B. L. Dou, Hydrogen generation from chemical looping reforming of glycerol by Ce-doped nickel phyllosilicate nanotube oxygen carriers, *Fuel* 222 (2018) 185–192.
- [2] G.W. Huber, S. Iborra, A. Corma, Synthesis of transportation fuels from biomass: Chemistry, catalysts, and engineering, *Chem. Rev.* 106 (2006) 4044–4098.
- [3] M.M. Abu-Omar, K. Barta, G.T. Beckham, J.S. Luterbacher, J. Ralph, R. Rinaldi, Y. Roman-Leshkov, J.S.M. Samec, B.F. Sels, F. Wang, Guidelines for performing lignin-first biorefining, *Energy Environ. Sci.* 14 (2021) 262–292.
- [4] Y. Liu, L.G. Chen, T.J. Wang, Q. Zhang, C.G. Wang, J.Y. Yan, L.L. Ma, One-pot catalytic conversion of raw lignocellulosic biomass into gasoline alkanes and chemicals over LiTaMoO<sub>6</sub> and Ru/C in aqueous phosphoric acid, *ACS Sustain. Chem. Eng.* 3 (2015) 1745–1755.
- [5] Z. Xiong, J.H. Guo, W. Chaiwat, W. Deng, X. Hu, H.D. Han, Y.J. Chen, K. Xu, S. Su, S. Hu, Y. Wang, J. Xiang, Assessing the chemical composition of heavy components in bio-oils from the pyrolysis of cellulose, hemicellulose and lignin at slow and fast heating rates, *Fuel Process. Technol.* 199 (2020), 106299.
- [6] C.Z. Li, X.C. Zhao, A.Q. Wang, G.W. Huber, T. Zhang, Catalytic transformation of lignin for the production of chemicals and fuels, *Chem. Rev.* 115 (2015) 11559–11624.
- [7] S.S. Wong, R.Y. Shu, J.G. Zhang, H.C. Liu, N. Yan, Downstream processing of lignin derived feedstock into end products, *Chem. Soc. Rev.* 49 (2020) 5510–5560.
- [8] W. Schutyser, T. Renders, S. Van den Bosch, S.F. Koelewijn, G.T. Beckham, B. F. Sels, Chemicals from lignin: an interplay of lignocellulose fractionation, depolymerisation, and upgrading, *Chem. Soc. Rev.* 47 (2018) 852–908.
- [9] R.Y. Shu, R.X. Li, B.Q. Lin, C. Wang, Z.D. Cheng, Y. Chen, A review on the catalytic hydrodeoxygenation of lignin-derived phenolic compounds and the conversion of raw lignin to hydrocarbon liquid fuels, *Biomass Bioenergy* 132 (2020), 105432.
- [10] B. Yan, X. Lin, Z. Chen, Q. Cai, S. Zhang, Selective production of phenolic monomers via high efficient lignin depolymerization with a carbon based nickel-iron-molybdenum carbide catalyst under mild conditions, *Bioresour. Technol.* 321 (2021), 124503.
- [11] L. Li, J.H. Kong, H.M. Zhang, S.J. Liu, Q. Zeng, Y.Q. Zhang, H. Ma, H.Y. He, J. X. Long, X.H. Li, Selective aerobic oxidative cleavage of lignin C-C bonds over novel hierarchical Ce-Cu/MFI nanosheets, *Appl. Catal. B Environ.* 279 (2020), 119343.
- [12] X.P. Ouyang, T. Ruan, X.Q. Qiu, Effect of solvent on hydrothermal oxidation depolymerization of lignin for the production of monophenolic compounds, *Fuel Process. Technol.* 144 (2016) 181–185.
- [13] R.Y. Shu, J.X. Long, Z.Q. Yuan, Q. Zhang, T.J. Wang, C.G. Wang, L.L. Ma, Efficient and product-controlled depolymerization of lignin oriented by metal chloride cooperated with Pd/C, *Bioresour. Technol.* 179 (2015) 84–90.
- [14] X.M. Dou, X. Jiang, W.Z. Li, C.F. Zhu, Q.C. Liu, Q. Lu, X.S. Zheng, H.M. Chang, H. Jameel, Highly efficient conversion of Kraft lignin into liquid fuels with a Co-Zn-beta zeolite catalyst, *Appl. Catal. B Environ.* 268 (2020), 118429.
- [15] R.Y. Shu, Y. Xu, L.L. Ma, Q. Zhang, C. Wang, Y. Chen, Controllable production of guaiacols and phenols from lignin depolymerization using Pd/C catalyst cooperated with metal chloride, *Chem. Eng. J.* 338 (2018) 457–464.
- [16] R.Y. Shu, B.Q. Lin, J.T. Zhang, C. Wang, Z. Yang, Y. Chen, Efficient catalytic hydrodeoxygenation of phenolic compounds and bio-oil over highly dispersed Ru/TiO<sub>2</sub>, *Fuel Process. Technol.* 184 (2019) 12–18.
- [17] S. Van den Bosch, W. Schutyser, R. Vanholme, T. Driessen, S.F. Koelewijn, T. Renders, B. De Meester, W.J.J. Huijgen, W. Dehaen, C.M. Courtin, B. Lagrain, W. Boerjan, B.F. Sels, Reductive lignocellulose fractionation into soluble lignin-derived phenolic monomers and dimers and processable carbohydrate pulps, *Energy Environ. Sci.* 8 (2015) 1748–1763.
- [18] B.W. Luo, Z.X. Huang, R.Y. Shu, Y. Cheng, Z.P. Tian, C. Wang, Y. Chen, Effects of metal site and acid site on the hydrogenolysis of cornstarch in supercritical ethanol during lignin-first fractionation, *Sustain. Energy Fuel* 5 (2021) 6097–6106.
- [19] Q.Z. Ma, Q.Y. Liu, W.Z. Li, L.L. Ma, J.D. Wang, M.H. Liu, Q. Zhang, Catalytic depolymerization of lignin for liquefied fuel at mild condition by rare earth metals loading on CNT, *Fuel Process. Technol.* 161 (2017) 220–225.
- [20] M.J. Fan, C. Li, Y.F. Sun, L.J. Zhang, S. Zhang, X. Hu, In situ characterization of functional groups of biochar in pyrolysis of cellulose, *Sci. Total Environ.* 799 (2021), 149354.
- [21] A.Q. Li, K. Shen, J.Y. Chen, Z. Li, Y.W. Li, Highly selective hydrogenation of phenol to cyclohexanol over MOF-derived non-noble Co-Ni@NC catalysts, *Chem. Eng. Sci.* 166 (2017) 66–76.
- [22] S. Wang, W. Gao, L.P. Xiao, J. Shi, R.C. Sun, G. Song, Hydrogenolysis of biorefinery corncob lignin into aromatic phenols over activated carbon-supported nickel, *Sustain. Energy Fuel* 3 (2019) 401–408.
- [23] Y. Wu, Y. Sun, K. Liang, Z. Yang, R. Tu, X. Fan, S. Cheng, H. Yu, E. Jiang, X. Xu, Enhancing hydrodeoxygenation of bio-oil via bimetallic Ni-V catalysts modified by cross-surface migrated-carbon from biochar, *ACS Appl. Mater. Interfaces* 13 (2021) 21482–21498.
- [24] W. Deng, X.P. Wang, C.H. Lam, Z. Xiong, H.D. Han, J. Xu, L. Jiang, S. Su, S. Hu, Y. Wang, J. Xiang, Evolution of coke structures during electrochemical upgrading of bio-oil, *Fuel Process. Technol.* 225 (2022), 107036.
- [25] M. Kumar, X. Xiong, Y. Sun, L.K.M. Yu, D.C.W. Tsang, D. Hou, J. Gupta, T. Bhaskar, A. Pandey, Critical review on biochar-supported catalysts for pollutant degradation and sustainable biorefinery, *Adv. Sustain. Syst.* (2020) 1900149.
- [26] G.H. Liu, Z.M. Zong, Z.Q. Liu, F.J. Liu, Y.Y. Zhang, X.Y. Wei, Solvent-controlled selective hydrodeoxygenation of bio-derived guaiacol to arenes or phenols over a biochar supported Co-doped MoO<sub>2</sub> catalyst, *Fuel Process. Technol.* 179 (2018) 114–123.
- [27] B. Liu, M. Yang, H.B. Chen, Y.J. Liu, D.G. Yang, H.M. Li, Graphene-like porous carbon nanosheets derived from salvia splendens for high-rate performance supercapacitors, *J. Power Sources* 397 (2018) 1–10.
- [28] Y. Hu, G. Jiang, G. Xu, X. Mu, Hydrogenolysis of lignin model compounds into aromatics with bimetallic Ru-Ni supported onto nitrogen-doped activated carbon catalyst, *Mol. Catal.* 445 (2018) 316–326.
- [29] T.J. Li, H.F. Lin, X.P. Ouyang, X.Q. Qiu, Z.C. Wan, In situ preparation of Ru@N-doped carbon catalyst for the hydrogenolysis of lignin to produce aromatic monomers, *ACS Catal.* 9 (2019) 5828–5836.
- [30] Z.Q. Yuan, J.X. Long, T.J. Wang, R.Y. Shu, Q. Zhang, L.L. Ma, Process intensification effect of ball milling on the hydrothermal pretreatment for corn straw enzymolysis, *Energy Convers. Manag.* 101 (2015) 481–488.
- [31] M.M. Mian, G.J. Liu, H.H. Zhou, Preparation of N-doped biochar from sewage sludge and melamine for peroxymonosulfate activation: N-functionality and catalytic mechanisms, *Sci. Total Environ.* 744 (2020), 140862.
- [32] F.H. Wang, Y.N. Wang, Y.J. Zhang, Y.M. Luo, H. Zhu, Highly dispersed RuCo bimetallic nanoparticles supported on carbon luo: enhanced catalytic activity for hydrogen generation from NaBH<sub>4</sub> methanolysis, *J. Mater. Sci.* 53 (2018) 6831–6841.
- [33] Z.H. Sheng, L. Shao, J.J. Chen, W.J. Bao, F.B. Wang, X.H. Xia, Catalyst-free synthesis of nitrogen-doped graphene via thermal annealing graphite oxide with melamine and its excellent electrocatalysis, *ACS Nano* 5 (2011) 4350–4358.
- [34] J. Okal, M. Zawadzki, W. Tylus, Microstructure characterization and propane oxidation over supported Ru nanoparticles synthesized by the microwave-polyol method, *Appl. Catal. B Environ.* 101 (2011) 548–559.
- [35] H.Z. Wang, W.Q. Guo, B.H. Liu, Q.L. Wu, H.C. Luo, Q. Zhao, Q.S. Si, F. Sseguya, N. Q. Ren, Edge-nitrogenated biochar for efficient peroxydisulfate activation: an electron transfer mechanism, *Water Res.* 160 (2019) 405–414.
- [36] Q.X. Ma, W.H. Chen, Z.H. Jin, L. Chen, Q.Y. Zhou, X. Jiang, One-step synthesis of microporous nitrogen-doped biochar for efficient removal of CO<sub>2</sub> and H<sub>2</sub>S, *Fuel* 289 (2021), 119932.
- [37] T.J. Li, H.F. Lin, X.P. Ouyang, X.Q. Qiu, Z.C. Wan, T. Ruan, Impact of nitrogen species and content on the catalytic activity to C–O bond cleavage of lignin over N-doped carbon supported Ru-based catalyst, *Fuel* 278 (2020), 118324.
- [38] B.Y. Du, C. Liu, X. Wang, Y. Han, Y.Z. Guo, H.M. Li, J.H. Zhou, Renewable lignin-based carbon nanofiber as Ni catalyst support for depolymerization of lignin to phenols in supercritical ethanol/water, *Renew. Energy* 147 (2020) 1331–1339.
- [39] B. Biswas, A. Kumar, R. Kaur, B.B. Krishna, T. Bhaskar, Catalytic hydrothermal liquefaction of alkali lignin over activated bio-char supported bimetallic catalyst, *Bioresour. Technol.* 337 (2021), 125439.
- [40] M. Wang, X.C. Zhang, H.J. Li, J.M. Lu, M.J. Liu, F. Wang, Carbon modification of nickel catalyst for depolymerization of oxidized lignin to aromatics, *ACS Catal.* 8 (2018) 1614–1620.
- [41] D. Wang, G.C. Li, C.H. Zhang, Z. Wang, X.B. Li, Nickel nanoparticles inlaid in lignin-derived carbon as high effective catalyst for lignin depolymerization, *Bioresour. Technol.* 289 (2019), 121629.
- [42] L. Gurrula, M.M. Kumar, A. Yerrayya, P. Kandasamy, P. Castano, T. Raja, G. Pilloni, C. Paek, R. Vinu, Unraveling the reaction mechanism of selective C9 monomeric phenols formation from lignin using Pd-Al<sub>2</sub>O<sub>3</sub>-activated biochar catalyst, *Bioresour. Technol.* 344 (2022), 126204.
- [43] Y.Y. Wang, L.L. Ling, H. Jiang, Selective hydrogenation of lignin to produce chemical commodities by using a biochar supported Ni-Mo<sub>2</sub>C catalyst obtained from biomass, *Green Chem.* 18 (2016) 4032–4041.
- [44] R.Y. Shu, J.X. Long, Y. Xu, L.L. Ma, Q. Zhang, T.J. Wang, C.G. Wang, Z.Q. Yuan, Q. Y. Wu, Investigation on the structural effect of lignin during the hydrogenolysis process, *Bioresour. Technol.* 200 (2016) 14–22.
- [45] J.X. Long, Y. Xu, T.J. Wang, Z.Q. Yuan, R.Y. Shu, Q. Zhang, L.L. Ma, Efficient base-catalyzed decomposition and in situ hydrogenolysis process for lignin depolymerization and char elimination, *Appl. Energy* 141 (2015) 70–79.